Chapter - 5

Energy Transduction System for Branched Flagellated Nanoswimmer

5.1   Introduction

In the previous chapter scaled up branched flagella was designed with objective to study enhanced propulsive force generation through planar motion of swimmer and optimization of system is done through DOE Taguchi analysis. The engrossment of nanorobots for various activities necessitates four fields: (a) energy storage, (b) energy transduction (c) control and (d) transmission [1]. Due to advancement in nanorobotics, on-board powering is the major concern for locomotion of nanoswimmer. On-board actuation of an artificial nanoswimmer is considered to be addressed by energy transduction mechanism. Energy can be harness from surrounding using energy of stochastic vibrations by electrostatic, electromagnetic and piezoelectric means. Energy harvesting, a process of capturing ambient energy and converting it into usable electricity, has been attracting more and more researchers' interest because of the limitations of traditional power sources. Increasing demands upon mobile devices such as wireless sensor networks, and the recent advent of the extremely low power electrical and mechanical devices such as micro-electro-mechanical systems (MEMS) and nanorobots necessitates powering and value of power requirement is mentioned in Table 5.1.

Table 5.1: Analogy of power requirements for different electronic devices [2]

Electronic Devices	Dimensions	Power Requirement
Server workstation	50cm - 90cm	Above 100W
Desktop PC	20 - 50cm	200 - 300W
Notebook PC	20 - 35cm	20 - 50W
Wireless sensor node	0.1 - 1cm	$100\mu W$ - 100mW
Nano-devices, Nanorobots	0.01 - $1\mu m$	1pW - $100\mu W$

Among all energy transduction mechanism, piezoelectric is emerging as a promising conversion transduction mechanism of energy harnessing for artificial nanoswimmer. In this context, in the present work, an elastic flagellum of a nanoswimmer is modeled as a cantilever beam and simulation study is done in COMSOL for the below listed parameters:

1. Novel design of branched flagellum is conceived, modeled and simulated. The effect of placement of branches/fins towards proximal end and distal end is studied.
2. Case 1: COMSOL simulation studies have been performed to compare the effect of primary and secondary branching on flagellum design in terms of stress and electric potential, when moving fluid is creating pressure on it.
3. Case 2: Fluid is kept stationary and planar oscillation is provided at one end of the cantilever beam design of energy harvester through prescribed velocity same as exhibited by micro-organisms to check how much energy flux and electric potential will be generated during planar oscillation.

In the present chapter, we first discuss about the energy harnessing process through piezoelectric mechanism. Various piezoelectric materials and their substantiality for energy conversion will be discussed. Literature reported on different designs of piezo harvester along with PVDF based energy harvester are presented in brief. Different designs of branched flagella are discussed for efficient generation of electrical components such as electric potential.

Locomotion design is combined efforts of chemists, biologists, physicists, pharmacists, engineers and mathematicians. Recent advancement in the field of nanotechnology enables to fabricate and design smarter nanomachines such as nanorobots which are capable of doing lots of task like repair of cells, nanosurgery [3], targeted drug delivery [4] and nano dentistry [5]. To propel artificial nanoswimmer, different propulsion mechanisms are developed to date like chemical actuation [6], [7], magnetic actuation [8], [9], ultrasonic actuation [10], thermal actuation mechanism [11] and bacterial actuation mechanism [12] as discussed in Chapter 2. Each and every actuation mechanism has some pros and cons [13], so the alternative of propulsion of an artificial nanoswimmer inside the human body is required. Scientists and engineers are mimicking natural biological bacteria such as cilia on *paramecium* for their design and fabrications of machines at nano levels for fluid mixing and pumping. The fabricated

cilia is actuated by external means such as electrostatic, optically driven cilia, hydrogel actuated artificial cilia, magnetic cilia, resonance actuated artificial cilia in the range of 10-100 Hz [14]. Magnetically actuated cilia may destruct the biological molecules in bio-samples whereas in electrostatic actuated cilia, electrolysis of solution occurs due to AC voltage manipulated cilia. The artificial cilia are fabricated on silicon base attached on one side of it and actuated by PZT micro-stage. The flow pattern around artificial cilia is studied by two dimensional simulation [15]. Mastigonemes on the surface of o*chromonas* are increasing the effective surface area which leads to increase in propulsive force. Different types of mastigonemes bearing flagella is presented in nature and *pantonematic* flagella shown schematically in Figure 5.1 is used in the present study to investigate energy generation for on-board actuation of an artificial nanoswimmer.
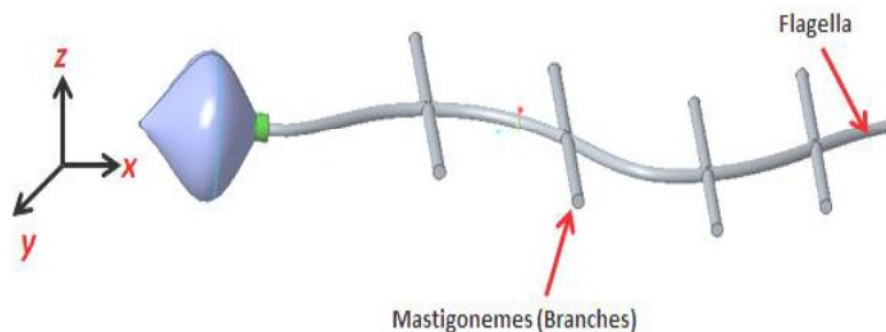

Figure 5.1: Schematic diagram of *pantonematic* flagella having mastigonemes on both sides of flagella surface [16]

Energy is classified in numerous ways such as mechanical, electrical, light, heat and chemical shown in Figure 5.2. Mechanical energy (motion) from the surrounding environment is being transduced in the form of electrical energy by electrostatic, electromagnetic and piezoelectric means and their respective power density is shown in Table 5.2. Piezoelectric technique seems more promising conversion technique because it requires piezoelectric materials to convert mechanical pressure or displacement directly in the form of electrical voltage. In the subsequent section, different piezoelectric materials are discussed briefly and their advantages and disadvantages are discussed to designed suitability of artificial nanoswimmer for biological applications.
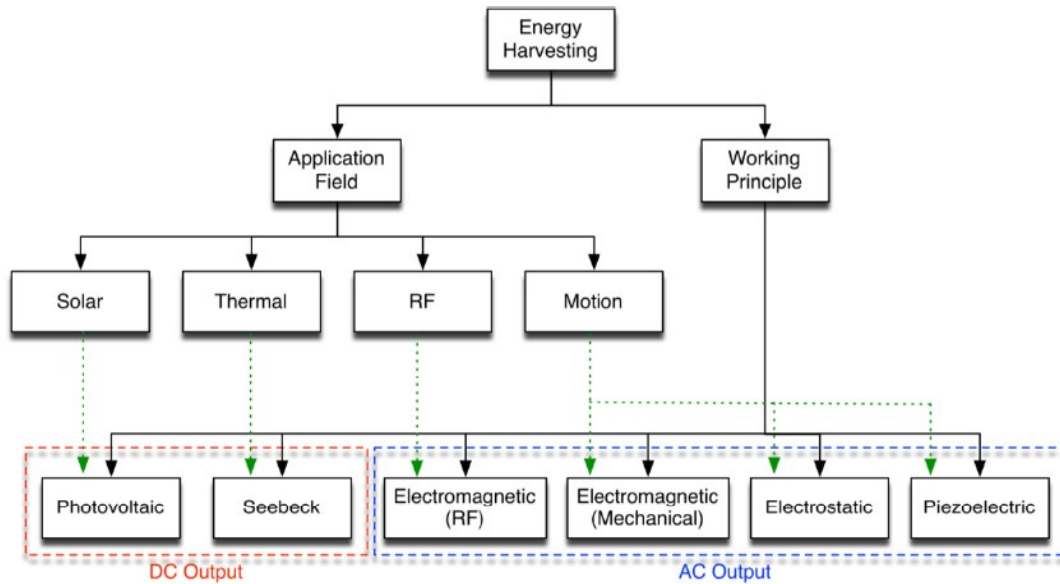
Figure 5.2: Classification of energy harnessing technologies [17]

Table 5.2: Various energy harnessing resource and their power density [18]

Energy Harnessing Resources	Power Density
Piezoelectric	$330\mu W/cm^3$
Vibration	$116\mu W/cm^3$
Thermoelectric	$40\mu W/cm^3$
Solar cells	$15mW/cm^3$

5.2 Energy Harvester Generators and Different Piezoelectric Materials

Energy transduction is the essential component in designing of nanorobots. A mechano-mechanical transducer is used to convert environmental vibrations into mechanical energy for on-board energy utilization such as circulation of blood of 1 m distance requires 10^{-6} pW of power while heart beat is offering power approximately 10^{-3} pW [19]. Among various kinds of energy, electricity is the most commonly used form because of it simply transformation into other types of energy. The term "Powering" generally implies conversion of any other form of energy into electrical energy. The most commonly used mechanism for conversion of mechanical energy

into electrical energy is electrostatic [20], piezoelectric [21], and electromagnetic [22]. The application of electromagnetic and electrostatic mechanisms as energy harvesting purpose possesses some limitations [23], [24]. The electromagnetic harvesters are providing low output voltage between 0.1 V to 0.2 V and larger in size which makes them impracticable to be used in MEMS [23]. It remains a challenge to design and fabricate an electromagnetic energy harvester in micro domain due to poor properties of magnet and coil. Electrodes are used as parallel plate capacitor in electrostatic energy harvester, which needs to be charge initially to start the conversion process [24]. In 1880, Jacques and Pierre Curie observed the effect of piezoelectricity. Piezoelectricity is the innate characteristics of the certain piezo-materials which makes it suitable for alternative energy harvester. The property of piezoelectric material such as conversion of ambient vibration into electrical form gained attentions of many researchers because it does not require any external power supply and can be useful in MEMS domain [22]. Piezoelectric generators have many advantages such as the mechanical energy required for conversion can be achieved from the environment, low cost, flexible and light weight. All these benefits of piezoelectric material can be utilized by designing a self-powered device for artificial nanoswimmer. Piezo-energy generators at micron scale have huge scope for research and applications in the today's world due to high energy density generation as shown in Table 5.3. In Table 5.3, piezoelectric energy harvester is showing the high value of energy per unit volume as comparison to electrostatic and electromagnetic.

Table 5.3: Comparison of energy harvester in terms of energy density [25]

Types of Energy Harvester	Energy Density (mJcm^{-3})
Electrostatic	4
Electromagnetic	24.8
Piezoelectric	35.4

Piezo-energy generators are classified as direct and inverse piezoelectric generator. In direct piezoelectric energy harvester, mechanical strain is converted into electric potential while in case of inverse piezoelectric generator electric potential is applied as input which has been converted into mechanical strain as shown in Figure 5.3.
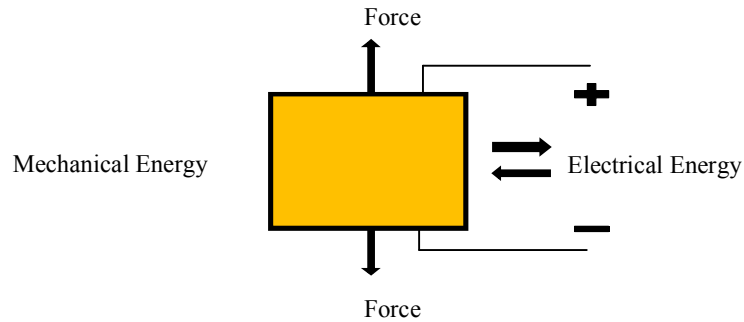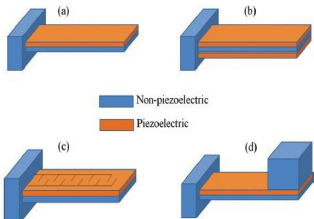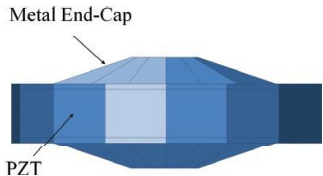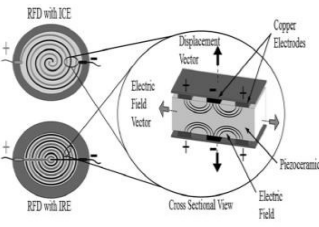
Force

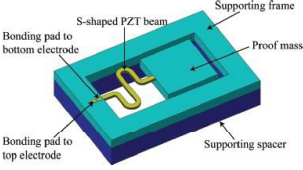Mechanical Energy   +   Electrical Energy   −

Force

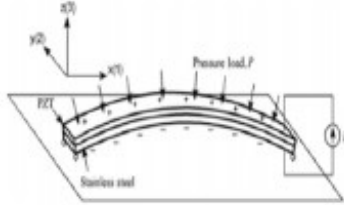**Figure 5.3: Schematic of direct and inverse piezoelectric effect**

Piezoelectricity can be seen in naturally occurring biological materials such as wood, bone and tendon, keratin, silk, enamel, myosin, Deoxyribonucleicacid (DNA) and Ribonucleicacid (RNA) [26]. Some of the ceramics which displays the piezoelectric effect are lead-zirconate-titanate (PZT), lead-titanate (PbTiO$_2$), lead-zirconate (PbZrO$_3$), and barium-titanate (BaTiO$_3$). PZT is the most frequently used piezoelectric ceramic because of high electromechanical coupling ability. However, PZT is an extremely brittle material and hence this presents limitations to the strain [27]. Polyvinylidenefluoride (PVDF) is another commonly used piezoelectric polymer which is flexible and can be employed in energy harvesting applications [28]. Over the last few years, zinc oxide (ZnO), piezo-ceramics such as PZT and piezoelectric polymers (PVDF) have been used for designing micro and nano systems [29]. PZT has low energy conversion efficiency [30] and it is fragile as compared to PVDF [31], [32] which makes it unsuitable to produce energy in alternating loads while PVDF is flexible, light weight, biocompatible and inexpensive [33]. Lead based piezoelectric materials are second alternative for energy harvesting but lead is a toxic material which may leave negative impression on the environment. Scientists are interested in synthesizing lead free piezoelectric material [34] and have developed the more flexible piezoelectric material. PVDF can be used in various applications of energy harnessing. Piezoelectric materials can with stand high strain, which leads to conversion of more mechanical energy into electrical energy. The biocompatible property [35] of PVDF makes it appropriate to be used for energy harnessing in human body for various applications like on board powering of nanoswimmer for various disease detection and drug delivery.

5.3 Literature on Various Structures of Piezoelectric Energy Harnessing Devices and PVDF Piezoelectric Generator

Various types of piezoelectric based energy harvesters are classified on the basis of shape. Cantilever beam structure is more attractive for energy harvesting purpose because of low resonance frequency and high average strain for a given applied force. The output of piezo-harvester can be controlled by changing the cantilever sensitivity. Researchers have increased the sensitivity of cantilever by changing the shape and dimensions [36] and utilized to design the branched flagella in the present thesis work. Some other configurations such as disc shape (cymbal and circular diaphragm), S-shaped cantilever, shell shape and stack type of piezoelectric energy harvester is shown in Table 5.4 along with its significant contribution.

Table 5.4: Different types of configuration of piezoelectric energy harvester [37]

Types of Configuration	Designs	Remarks
Cantilever		Produce large mechanical strain Simple in design Power output is maximized by proof mass. Used for low vibration energy harvesting.
Cymbal		Used for high impact forces applications Better efficiency than cantilever
Circular Diaphragm		Pre-stressing of circular diaphragm is done by attaching proof mass in the center. Power output in nano-watt is produced at smaller resonance frequency approximately 1.56KHz
S-shaped cantilever		Decreasing the stiffness of cantilever beam to attain low resonance frequency

Types of Configuration	Designs	Remarks
Shell Type		Better energy harvester than cantilever beam. Only used for torsional load.
Stack type		Used for large forces to generate larger amount of energy.

Piezoelectric material own crystalline structure, it means dipole moment characteristic is present inside it. When subjected to mechanical strain, dipole moment is altered and lead to electric charge generation. There are two modes of piezoelectric material d_{31} and d_{33} depending on the direction of force applied and voltage generated axis. In d_{31} mode, force or stress is applied in direction '1' and voltage is generated in direction '3'. While in d_{33} mode, both bending stress and respectively voltage is generated in direction '3' as shown in Figure 5.4. The theoretical evaluation of power generated from piezoelectric material due to applied force or pressure is given in literature [38]. The electrical energy E_e is given by equation (5.1).

$$E_e = VC \tag{5.1}$$

where, V is the voltage and C is the electric charge developed on piezoelectric film. Voltage and charge are given by equation (5.2) for beam elements are

$$V = \frac{Fg_{31}}{W}, \; C = \frac{FLd_{31}}{T} \tag{5.2}$$

where, F is the force developed on the piezo surface, W and T are the width and thickness of the cantilever beam, g_{31} and d_{31} are the stress and strain constant of piezoelectric material. The electric power of piezo cantilever beam due to applied frequency (Hz) is obtained by equation (5.3).

$$P_e = VCf = \sigma_{31}^2 d_{31} g_{31} TWLf \tag{5.3}$$

In the above equation σ_{31} is the stress of the piezoelectric cantilever beam. Theoretically, the external stress σ_{33} in 33-mode, generates electric field E and is proportional to the piezoelectric voltage coefficient g_{33} given in equation (5.4) and correspondingly output voltage can be expressed as V by reducing the problem as $E = V/L$ and $\sigma = \varepsilon Y$, where Y is the Young's modulus of elasticity of material and L is the length of the piezoelectric material.

$$E_{33} = g_{33}\sigma_{33}, \quad V = g_{33}\varepsilon YL \tag{5.4}$$

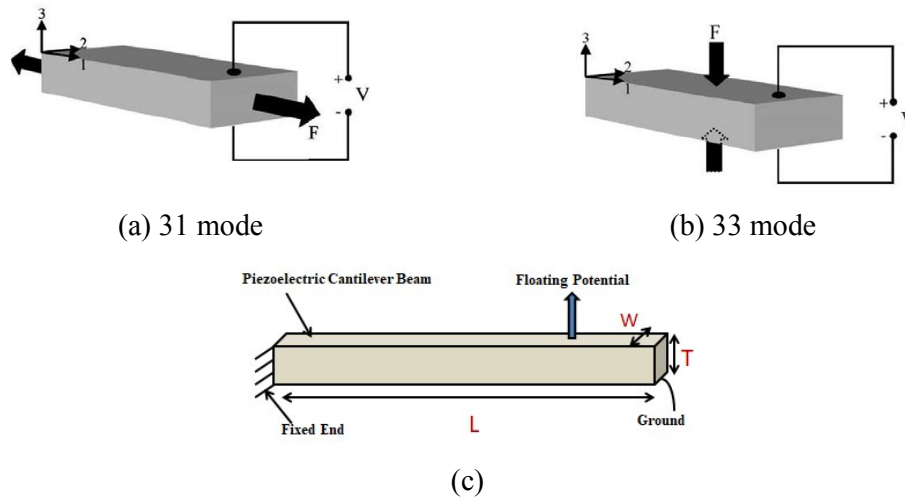(a) 31 mode   (b) 33 mode

(c)

Figure 5.4: (a) and (b) shows the d$_{31}$ and d$_{33}$ modes of piezoelectric film, (c) Piezoelectric cantilever beam fixed at one end and electric potential generated at upper surface of beam due to force application

Energy harvesting using piezoelectric generator at low frequency input becomes a popular research area between researchers over last several decades. This put forth a challenge for the researchers to optimize the energy output along with design and piezoelectric material based energy harvester. Piezoelectric materials are divided into four groups like ceramics, composites, single crystals and polymers. Piezoelectric polymer is getting more attention in the field of biomedical application due to flexibility can sustain high strain. PVDF is the mostly used polymer. It is made up of repeating unit of (CH_2-CF_2) and is semi-crystalline in nature. Piezoelectric polymer is flexible, lighter in weight and low piezoelectric constant than mostly used PZT ceramics. Because of flexibility and small volume of PVDF it is widely used in back packs and in sole of shoes. The available literature on generation of electric output through PVDF is tabulated in Table 5.5.

Table 5.5: Literature on achievement in the field of PVDF piezoelectric generator

Year/Author	Design	Input/ Output
1998- Kendall [39]	PVDF sheet	0.6 mW power is generated on exciting at 2 Hz by PVDF sole in shoe.
2001- Taylor et al. [40]	Eel shape- Length 9.5 inches, width 3 inches and thickness 150 μm.	Input Velocity- 0.35, 0.5 and 0.67 m/s and correspondingly output voltage is measured as 877, 1024 and 1310 V.
2004- Pobering and Schwesinger [41]	PVDF Flag	Power output is created 11-32 Wm^{-2} at flow velocity of 2 ms^{-1}.
2007- Sodano et al. [42]	Two PVDF strap backpack	At 50-lb load, 10 mW of power is produced.
2009- Chang et al. [43]	PVDF-CNT composite nano-fibers using electro spinning.	Voltage generated 8.5 mV and approximately output power is 7.2 pW. Reinforce the CNT to increase the electrical conductivity.
2010- Hansen et al. [44]	PVDF nano-fibers	Output voltage 50 mV measured inside a glucose biofuel cell.
2014- Mutsuda et al. [45]	Multicore PVDF sheets	Generate 27 V at 11.3 Hz in air environment.
2017- Proto et al. [46]	PVDF film transducer	RMS value of power output measured was in the range of 0.1-10 μW.
2018- Li et al. [47]	PVDF/ graphene oxide composite nanofiber film	The force of the exciter was set as 10 N and 21 V output is generated.
2018- Nain et al. [48]	PVDF based cantilever beam in nanometers	Generated 188nV at fluidic velocity 80 μm/s.
2019- Mokhatri et al. [49]	Braided PVDF yarns	Compression and bending of PVDF yarns generates the output voltage of 380 mV with power density 29.62 $μWcm^{-3}$.

The available literature on PVDF energy generator is available for non-biomedical applications such as MEMS for low frequency input. In the present thesis, the energy harnessing device for primary and secondary branched flagellated artificial nanoswimmer is simulated using COMSOL to see the effect of various designs of branched flagella on the induced stress as well as electric potential. The piezoelectric

material based nanoswimmer is easy to fabricate in cantilever beam shape, so we simulate the model in the following section while considering its future biomedical applications such as targeted drug delivery and nano-surgeries.

5.4 Primary and Secondary Branched Flagellated Artificial Nanoswimmer: Design and Simulation

In nature various kinds of eukaryotic and prokaryotic microorganism exist, which are using cilia and flagella to locomote themselves [50]. The motivation of present work comes from the existence of cilia and mastigonemes. The presence of cilia helps in the motion of cell like *paramecium*. We can utilize the motion of cilia like structures for production of energy which can be used further for propulsion of nanoswimmer. The structure's quintessential requirement is piezoelectric behavior which is to be used for energy transduction. In this work, the basic design for on-board energy harnessing for nanoswimmer is obtained using simple beam shaped flagella like structure of PVDF fixed at one end.

In pursuit to harness energy from piezoelectric material, a cantilever beam based piezoelectric energy harvesting device has been proposed by researchers to delve substantial energy from ambient vibration [51], [52]. Mathematical modeling has been used to see the effect of geometric parameters such as beam length, width and thickness on the voltage generation and power [53]. A simulation approach is used to prove the concept of voltage generation on piezoelectric device inside flowing fluid channel. In almost all the attempts [54], [55] of energy harnessing in different fluid mediums such as water and air, studies have been performed at Reynolds number greater than one as discussed in Chapter 2 and Table 5.5. In the context, the present study deals with the simulation of branched nanoswimmer in fluid with Reynolds number less than 1 [56]. The output performance is measured in terms of stresses and electric potential developed on piezoelectric based nanoswimmer. It is of interest to determine how the variation in branched ciliary/mastigonemes density, their design and placement will affect the generation of energy on piezoelectric artificial nanoswimmer. In this context, in the present work, an elastic flagellum of a nanoswimmer is modeled as a cantilever beam and simulation study is done in COMSOL. Novel design of branched flagellum is conceived, modeled and simulated. COMSOL simulation studies have been performed to compare the effect of primary and secondary branching in flagellum design in terms of

stress and electric potential. An enhanced stress allows for larger efficiency of conversion mechanism and therefore branching of flagellum can be pivotal in increasing on-board harnessing of energy for propulsion of nanorobots.

5.4.1 Design and simulation of actuation scheme of primary branched artificial nanoswimmer

The schematic of proposed design is shown in Figure 5.5. Nanoswimmer constitute of a head and tail (i.e. flagella). Growth of mastigonemes is envisaged on flagella which may be branched or unbranched as shown in Figure 5.5. Corresponding to one branched flagella, a model design is shown in Figure 5.5 (b). The beam corresponds to flagella and branches are like mastigonemes on flagella. The beam body is fixed at one end which denotes the flagella-branches joint in Figure 5.5 (a).
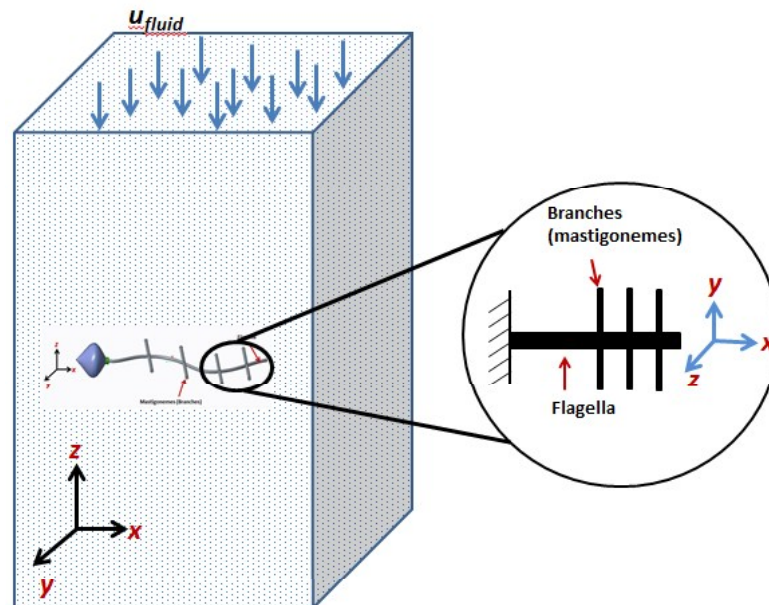

Figure 5.5: (a) Schematic of nanoswimmer and (b) Mapped model of branched flagella for simulation

Simulation of energy transduction system for artificial nanoswimmer is carried out in COMSOL 5.2@ multiphysics finite element software. The problem involves a fluid structure interaction (FSI) where the flow of fluid will results in deformation of piezoelectric structure which helps in generation of electric potential due to tail. Fluid structure interaction (FSI) and solid mechanics modules are coupled together to study the effect of flowing fluid velocity on piezo based flagellated nanoswimmer. To maintain flexural rigidity of the nanoswimmer the geometric parameters, chosen for the simulation

are similar to the cilia present on the surface of *paramecium* and [57], [58]. Simulation steps are shown in Figure 5.6 and given in Appendix II.
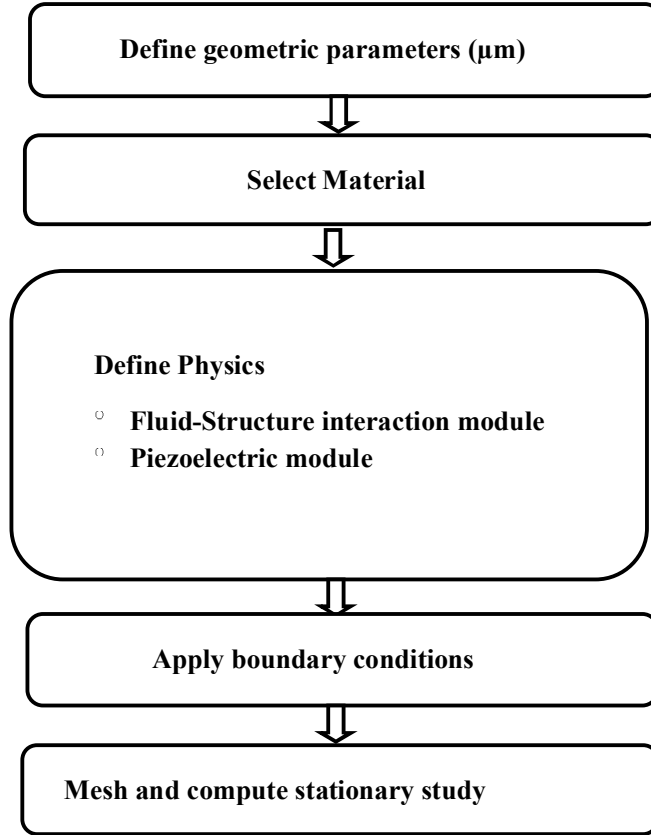
```
┌─────────────────────────────────────────────┐
│      Define geometric parameters (µm)         │
└─────────────────────────────────────────────┘
                     ⇩
┌─────────────────────────────────────────────┐
│               Select Material                 │
└─────────────────────────────────────────────┘
                     ⇩
┌─────────────────────────────────────────────┐
│                                               │
│   Define Physics                              │
│    ○  Fluid-Structure interaction module      │
│    ○  Piezoelectric module                    │
│                                               │
└─────────────────────────────────────────────┘
                     ⇩
┌─────────────────────────────────────────────┐
│           Apply boundary conditions           │
└─────────────────────────────────────────────┘
                     ⇩
┌─────────────────────────────────────────────┐
│       Mesh and compute stationary study       │
└─────────────────────────────────────────────┘
```

Figure 5.6: Simulation process flow for energy transduction system of nanoswimmer

The model geometry consists of cantilever beam structure acting as flagella is made up of PVDF piezoelectric material inside a fluidic channel. In FSI module, a parabolic velocity profile is introduced as inlet boundary condition [59]. The inflow velocity of fluid is applied perpendicular to the piezoelectric beam kept inside the fluidic chamber, which develop the stresses on the beam due to fluid flow pressure and governed by Navier-Stokes equation (5.5).

$$\rho(u_{fluid} \bullet \nabla)u_{fluid} = \nabla \bullet [-pI + \mu(\nabla u_{fluid} + (\nabla u_{fluid})^T] + F \qquad (5.5)$$

where ρ is the density of fluid, u_{fluid} is the velocity of fluid, p is the pressure, I is the identity tensor, μ is the viscosity of fluid and F is the total force acting on the surface of structure. When Reynolds number is zero, the fluid motion is dominated by Stokes

equation [60] by reducing equation (5.5) into (5.6), where inertial forces are neglected and viscous forces are dominated:

$$-\nabla p + \mu \nabla^2 u_{fluid} = 0 \qquad (5.6)$$

Laminar flow is used to compute the velocity and pressure field through continuity equation of motion and momentum equation of motion. For constant density of medium continuity equation (5.7) is

$$\rho \nabla \bullet (u_{fluid}) = 0 \qquad (5.7)$$

If the inlet boundary is closer to the solid structure, it may affect the flow pattern, so, the dimensions of the fluid domain are chosen in such a way to avoid the wall effects. The beam is fixed at one end and is representing flagella. The fluid velocity is chosen in the range of velocity 5 µm.sec^{-1} to 8 µm.sec^{-1} to maintain low Reynolds number regime and to mimic swimming speed of natural bacteria such as *E.coli* and *paramecium* (2 µm.sec^{-1} to 500 µm.sec^{-1}) [61], [62]. The laminar fluid flow is maintained in the container of size 300 µm×150 µm×150 µm in which piezoelectric beam is placed. The velocity of liquid will leads to generation of stress on the cantilever beam which in turns develops electric potential on the piezoelectric beam due to fluidic pressure.

Material properties of PVDF considered for simulation are shown in Table 5.6. The dimensions of energy harnessing branched flagellated artificial nanoswimmer systems are shown in Table 5.7. Inlet velocity is varied between 5-8 µms^{-1} to maintain Reynolds number less than 1 inside the micro channel [56]. The pressure applied by flowing fluid deforms the elastic structure. In quest of material, PVDF is proved to be more feasible piezo-material because of its biocompatibility with human body and different body fluids [35]. In the design, flagella are considered as a beam and branching are attached as mastigonemes to flagella i.e. main body (refer Figure 5.5).

In FSI module, a parabolic velocity profile [59] u_{fluid} is introduced as inlet boundary condition represented by equation (5.8) mentioned below:

$$u_{fluid} = \frac{U \times 16 \times (H - Y) \times (H - X) \times Y \times X}{H^4} \qquad (5.8)$$

where, *U* is the mean velocity of water defined to maintain Reynolds number less than 1 and to sustain laminar flow regime. *H* is the height of the outer domain in which fluid is flowing i.e. 300 μm to avoid wall effects. *XY* is the plane in which fluid is entering.

Table 5.6: Material properties for energy harnessing design of artificial nanoswimmer

Material Properties	PVDF
Young's Modulus (GPa)	2
Density (kg.m^{-3})	1780
Poisson's ratio	0.3

To study the voltage generation, fluidic pressure developed on polymer surface is defined as boundary load in piezoelectric module. The lower surface of the cantilever beam is grounded and floating potential on the upper surface is applied to see the effect of fluid flow on piezoelectric cantilever beam as shown in Figure 5.4(c). The model is meshed with physics controlled mesh with element size normal. The average von Mises stress generated on the beam surface is within the permissible limit of materials for PVDF (PVDF Young's Modulus 2 GPa).

Table 5.7: Geometric parameters of proposed design of on-board energy harnessing system for artificial nanoswimmer

	Length (μm)	Width (μm)	Thickness (μm)
Beam	50	0.25	0.25
Branches	5	0.025	0.025

In Chapter 4, we have considered three orientations 90°, 60° and 120° of branches on flagella surface. The experiments are performed and it was observed that maximum propulsive force is measured for 90° oriented branches and then 60° and 120°. Here, we are considering only 90° and 60° oriented branches for simulation by varying the number of branches and placement of branches on flagella surface.

Four sets of designs are explored for energy transduction system of an artificial nanoswimmer by varying the number of branches from 2 to 6. The first design is

straight beam representing mastigonemes with four variations in number of branches and their placement (which is towards fixed end) Refer Figure 5.7, Design 1(a). Second design is similar to first but with placement of fins at distal end from fixed end (Refer Figure 5.7, Design 1(b)). In third and fourth design (Figure 5.7, Design 2(a) and Design 2(b)), the fins are placed at nearer and distal end with respect to fixed end but are tilted with beam axis. The orientation of branches is taken 90° and 60° on flagella surface. The spacing between branches is kept constant 0.05 μm. Simulations are carried out to investigate the effects of fin density and tilt angle on stressing of beam and eventually transduction to electric potential by piezoelectric effect.

Design 1(a)

Design 1(b)
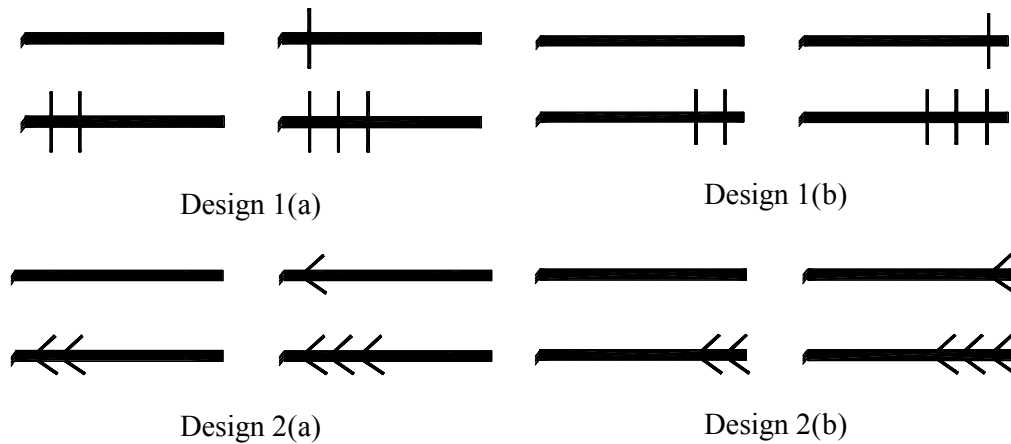
Design 2(a)

Design 2(b)

Figure 5.7: Different designs of energy harnessing system of an artificial nanoswimmer

5.4.2 Results and discussion

The patches of mastigonemes are simulated, in the form of branches attached to the beam (flagella) inside the fluidic channel as shown in Figure 5.8(a). The water (density 1000 Kgm^{-3} and dynamic viscosity 0.001 Pas) is flowing inside the micro-channel at different velocity (5 μms^{-1} to 8 μms^{-1}) to maintain laminar flow regime. The piezo based energy harnessing design is enduring deformation from undeformed phase as shown in Figure 5.8(b) due to fluidic pressure is applied as boundary load on the surface of the beam. The key interest lies in to analyze the effect of flowing fluid on generation of electric potential.
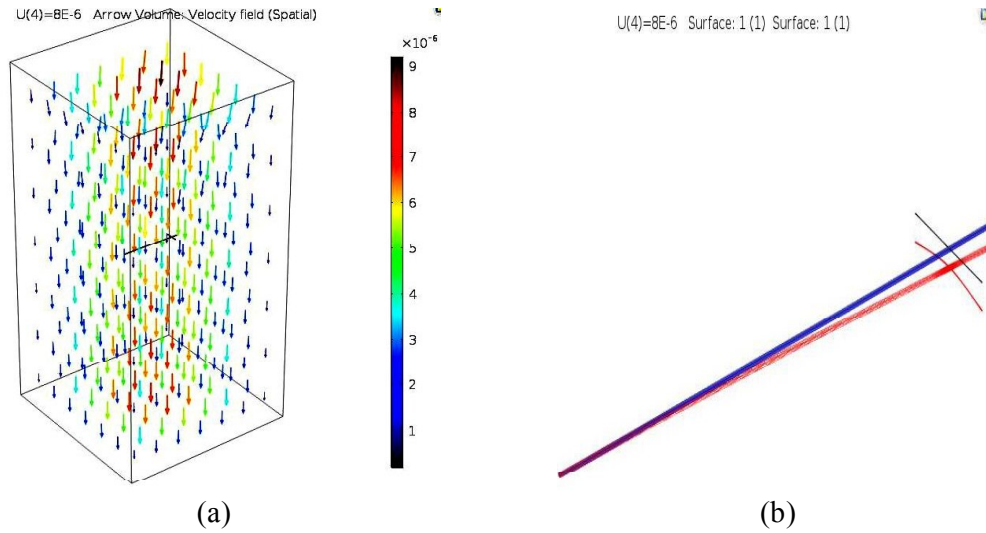
(a)   (b)

Figure 5.8: (a) Incompressible fluid is flowing inside a micro channel over branched flagella, (b) deflection of branched beam at fluid velocity 8 µms⁻¹

The simulation results of line average stress towards fixed end are plotted in Figure 5.9. The plots are family of curves for different designs (with varying number of fins) and presents stress on *y*-axis and flow velocity on *x*-axis. The pressure of fluid velocity on the structure is considered as load and the stress are developed on the branched flagellated artificial nanoswimmer and given by equation (5.9).

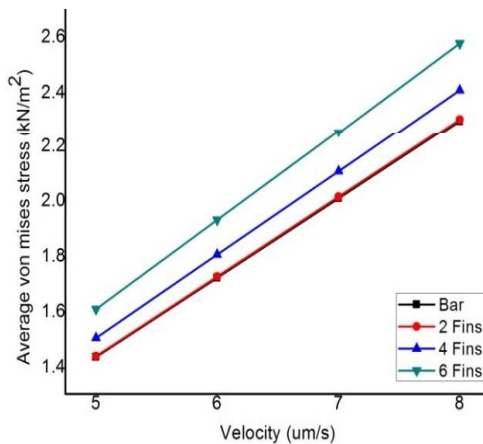$$\text{von Misesstress}(N/m^2) = \sqrt{3 \times J} \tag{5.9}$$

where *J* is the second invariant of stress deviator. From the results plotted in Figure 5.9, it is observed that as the number of fins increases on beam, the stress will also increase. This validates the hypothesis that branching will increase (amplify) the stress. The highest stress developed is order of 3800 Nm⁻² which is quite low when compared against allowable stress in PVDF ($\sigma_{\text{allowabe (PVDF)}}$ 1.7 to 8.3 GPa) [35].
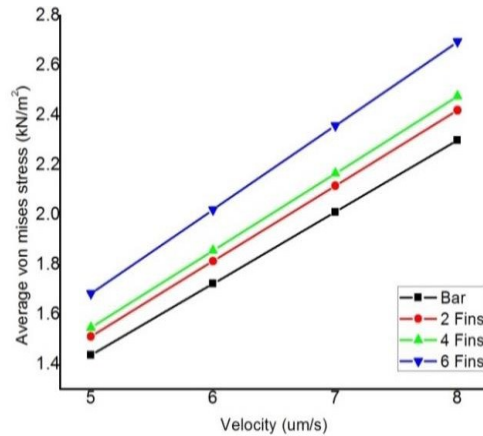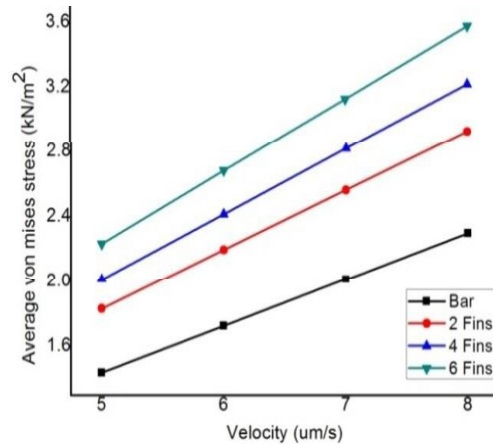
Design 1(a): Average von Mises stress
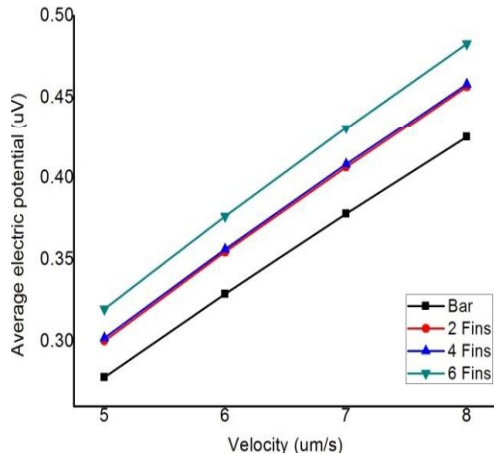v/s velocity
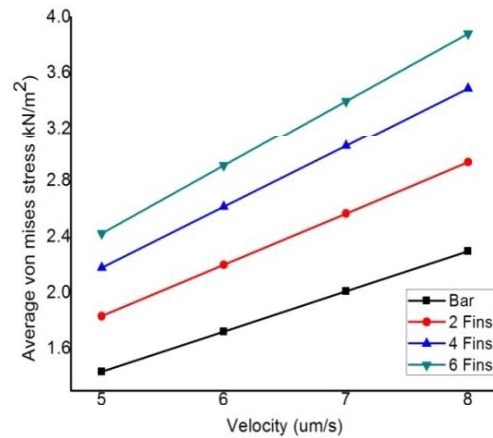
Design 1(b): Average von Mises stress
v/s velocity

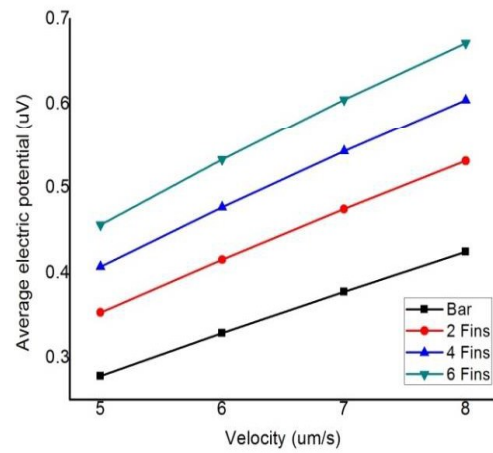Design 2(a): Average von Mises stress
v/s velocity

Design 2(b): Average von Mises stress
v/s velocity

Figure 5.9: Stress variation with increasing number of fins for four different designs

The simulation model is developed using piezoelectric module where electrostatic module is coupled to generate electric potential when the beam is deformed due to fluidic pressure load application. The stresses are further converted into electric potential using electrostatic module and corresponding to each stress graph, electric potential variations are plotted as a function of velocity in Figure 5.10. The highest electric potential developed is of the order of 0.7 µV for 6 branched flagella towards distal end at 90° orientation. This is quite promising and further branching can enhance the energy harnessing and transduction of fluid flow energy.
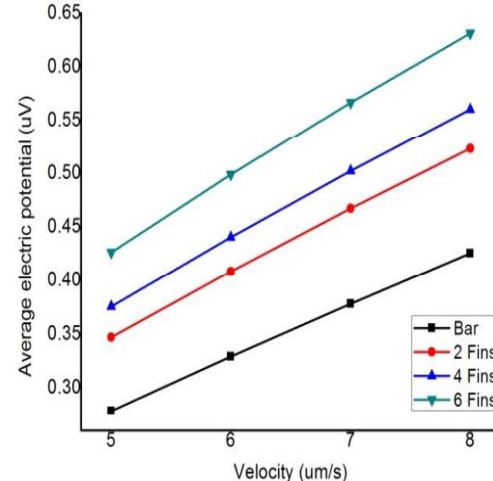
Design 1(a): Average electric potential
v/s velocity

Design 1(b): Average electric potential
v/s velocity
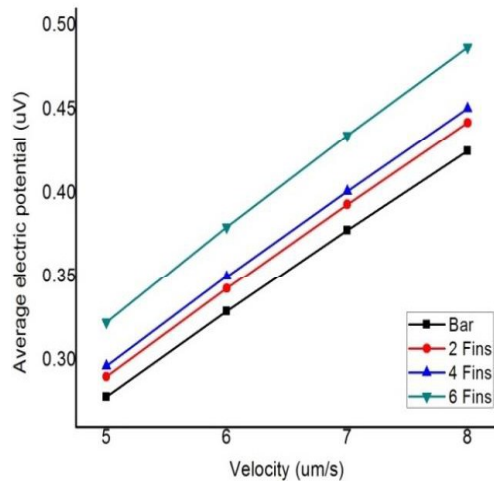
Design 2(a): Average electric potential
v/s velocity

Design 2(b): Average electric potential
v/s velocity

Figure 5.10: Variation in electric potential with increasing number of fins for four different designs

The percentage increase in von Mises stress is calculated for each design and compared with that of simple beam without branches. Calculated values for percentage increase in von Mises stress and electric potential are shown in Table 5.8. Design 1(b) (Figure 5.7) is providing best results by giving maximum stress with an increase of 68.95% and corresponding electric potential increase of 60.65%. Design 1 (b) and Design 1 (c) is providing better results in comparison to other designs of Figure 5.7. Because there will be less drag when branches are present towards free end of beam and results in terms of electric potential will get amplify. 90° orientation of branches is showing 60.65% increase in electric potential as comparison to 60° orientation of branches on flagella

surface. As mentioned in literature [63], 90° orientation of branches (mastigonemes) on flagella surface is more efficient in generating propulsive velocity because effective surface area is increased. The same concept is applied here to design and simulate piezo based branched flagella to study electric potential generation which can be utilized for on-board energy transduction of artificial nanoswimmer.

Table 5.8: Comparison of percentage increase in stress for different designs of energy transduction system

Designs	Percentage increase in von Mises stress	Percentage increase in electric potential
Design 1 (a)	17.25%	14.13%
Design 1 (b)	68.95%	60.65%
Design 2 (a)	12.13%	15.13%
Design 2 (b)	55.52%	50.47%

The deformation of a branched beam with 6 fins attached to it (refers Figure 5.7, design 1(b)) at velocity 8 μms^{-1} is illustrated in Figure 5.11. The maximum displacement is indicated towards free end of the beam. The magnitude of the displacement is increased linearly as number of branches is increased on the beam at velocity 8 μms^{-1}. The maximum displacement observed in case of 6 branches at 90° orientation on flagella surface is 0.0137 μm. Maximum 6 primary branched flagellated nanoswimmer design is studied in the present work to investigate the effect of branches on electric potential generation.
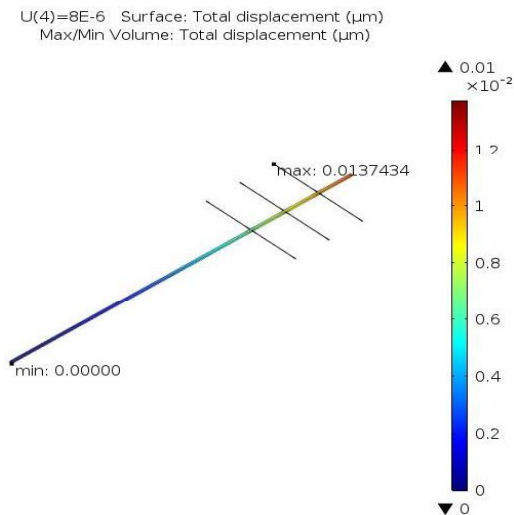

Figure 5.11: Maximum displacement for 6 fins of design 1(b) of figure 5.7

In the following section, effect of secondary branches placed on primary branch surface (fibers on mastigonemes) is attempted to study further enhancement of electric potential development in comparison to same design of primary branched flagellated nanoswimmer.

5.5 Effect of Secondary Branching on Flagellated Artificial Nanoswimmer

In nature *ochromonas danica* is showing fibers on mastigonemes as shown in Figure 5.12(a). In present design of flagella, mastigonemes are arranged in the form of primary branches and secondary branches (fibers) on the simple cantilever beam made of PVDF piezoelectric material as shown schematically in Figure 5.12(b). The aim of the design is to study amplification in stress on the main trunk (flagella) due to secondary branching of structure which has been transduced in the form of electric potential due to piezoelectric effect. Simulations are carried out in COMSOL simulation software and design is considered to enhance the electric potential.
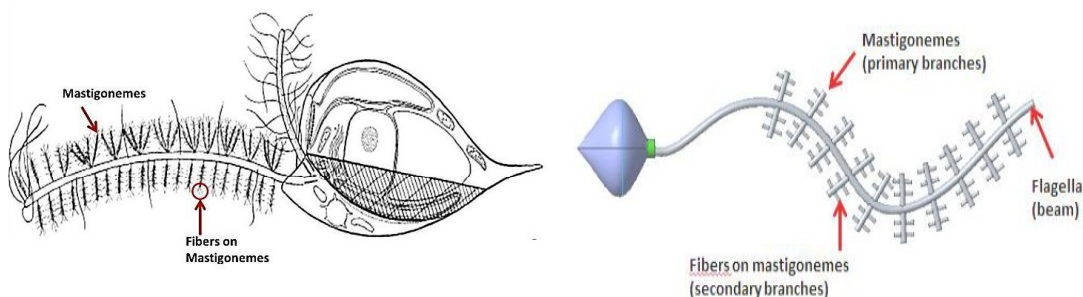

Figure 5.12: (a) *Ochromonas danica* showing fibers (secondary branches) on mastigonemes (primary branches) [64] **and (b) schematic diagram shows secondary branches on mastigonemes present on flagella surface**

5.5.1 Modelling of an secondary branched energy harnessing mechanism for artificial nanoswimmer

Investigations of different designs of actuation mechanism of artificial nanoswimmer are carried out to explore it's suitability for on-board energy transduction. The most appropriate method to design a nanoswimmer is to mimic natural bacteria consists of cilia and flagella as mode of propulsion. The flagella could be branched or unbranched as shown in Figure 5.13. The simple beam fixed at one end is representing flagella while numbers of primary branches (mastigonemes) are varying from 2 to 6 towards distal end.

In our previous analysis [65], the effect of primary branches was investigated it was observed that as number of primary branches are increased towards free end of beam, stress gets amplified leads to increase in electric potential. The design with primary branches at distal end (refer Figure 5.7 Design 1(b)) with respect to primary branches at fix end of beam seems more promising structure for energy harnessing purpose which needs to be explored further for secondary branching. The design shown in Figure 5.13, branches towards distal end are showing maximum amplification of electric potential approximately 60% through simulation [65]. It needs to investigate further to study the effect of secondary branches (static load) and fluidic pressure (dynamic load) for electric potential development on the main structure of beam flagella and is attempted in the subsequent section.
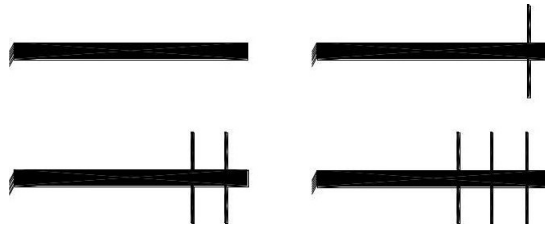

Figure 5.13: Model of unbranched and branched flagella

The numbers of primary branches are kept constant as 2 for initial study and number of secondary branches are varied from 4 to 8 to investigate the change in stress and electric potential. The dimensions of secondary branches are same as primary branch shown in Table 5.7. In 2 primary branches case, it is possible to maintain uniformity of placing secondary branches as shown in Figure 5.14. In 4 or 6 primary branches the gap between primary branches need to increase while placing secondary branches on each primary branch. The proposed designs for secondary branches are shown in Figure 5.14. The spacing between secondary branches is kept constant 0.05 μm and their dimensions are same as primary branches as shown in Table 5.7. The purpose of secondary branches are to scrutinized the further percentage increase in electric potential for same primary branched designed flagellated swimmer.
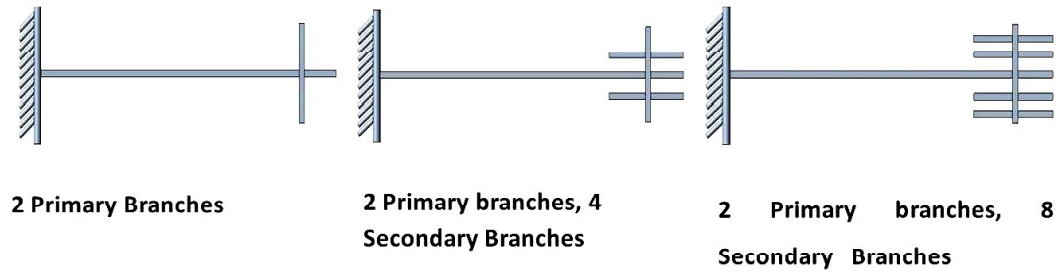
2 Primary Branches　　　　**2 Primary branches, 4**　　　　**2   Primary   branches   8**
　　　　　　　　　　　　　　　 Secondary Branches　　　　　 **Secondary Branches**

**Figure 5.14: Design of secondary branched flagellated artificial nanoswimmer
(numbers of primary branches are constant)**

5.5.2　Results and discussion

A nanostructure device made up of piezoelectric material is investigated that can be used to convert mechanical energy into electrical energy for self-powering micro/nano-device such as in medical diagnostic applications and *in-vivo* drug delivery system [24]. In human body, heart beat and blood flow can be used as mechanical energy which helps to generate power for implantable device.

Biocompatible energy harnessing device for artificial nanoswimmer is modeled and its electric potential is estimated. The piezo generators consist of a main cantilever beam with primary and secondary branching to get more electric potential. When fluid enters perpendicular to the beam of the structure it generates stress on it. The incompressible fluid such as water (density 1000 Kgm^{-3} and dynamic viscosity 0.001 Pas) is flowing inside the micro-channel at different velocity (5 μms^{-1} to 8 μms^{-1}) to maintain laminar flow regime.

The simulation results of stress and electric potential are plotted for different designs of secondary branching structure at different velocity. From the results plotted in Figure 5.15, it is noticed that as number of secondary branches increases on the beam from 2 primary branches to 8 secondary branches, the stress will also increase. The amplification in stress due to secondary branching is studied. The maximum stress achieved is approximately 2700 Nm^{-2} which is low as compared to the permissible level of stress in PVDF ($\sigma_{allowable}$ (PVDF) 1.7 to 8.3 GPa) [35]. The stress and electric potential was calculated near the fixed end of the beam. To design on-board actuation scheme of branched flagellated artificial nanoswimmer, the results are always taken towards fixed

end of beam, so that electric potential is picked up at initial points and can be used for further locomotion. The electrostatic module is already coupled with piezoelectric module in COMSOL.
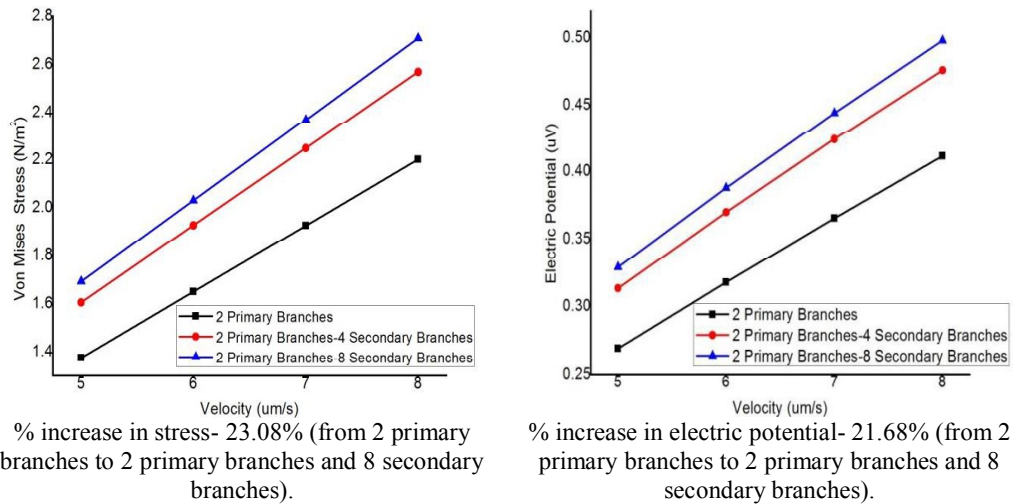

% increase in stress- 23.08% (from 2 primary branches to 2 primary branches and 8 secondary branches).

% increase in electric potential- 21.68% (from 2 primary branches to 2 primary branches and 8 secondary branches).

Figure 5.15: Variation in stress and electric potential on increasing secondary branches

Similar to each stress value electric potential variations are plotted as a function of fluid velocity. The maximum electric potential developed is in the order of 0.5 μV for 2 primary branches and 8 secondary branch designed nanoswimmer at 8 μms^{-1} of fluidic velocity. As varying velocities are applied on the different designs of nanoswimmer from 2 primary branches to 8 secondary branches design, increase in stress and electric potential was noticed as 23.08% and 21.68% which is tabulated above in the form of graphs as shown in Figure 5.15.

5.5.3 Effect of placement of secondary branches on 4 primary branched flagella surface

In the present study, 4 primary branches placed towards proximal end and distal end are considered. In Design 1(a), Design 1(b) and Design 1(c) (Figure 5.16) 4 and 8 secondary branches are positioned uniformly on 4 primary branches towards fixed end of beam. In Design 2, number of secondary branches is increased towards free end of beam. The gaps between primary branches are consistent for 4 secondary branched flagellated nanoswimmer (Design 1(b) and Design 2(b) (refer Figure 5.16)). When 8 secondary branches are placed at 4 primary branches design (Design 1 (c) and Design 2 (c) Figure 5.16) the gap between primary branches are increased twice the length of secondary

branches and to accommodate 8 secondary branches uniformly on primary branches. Modeling and designs of energy transduction mechanism is carried out in COMSOL multiphysics finite element software.
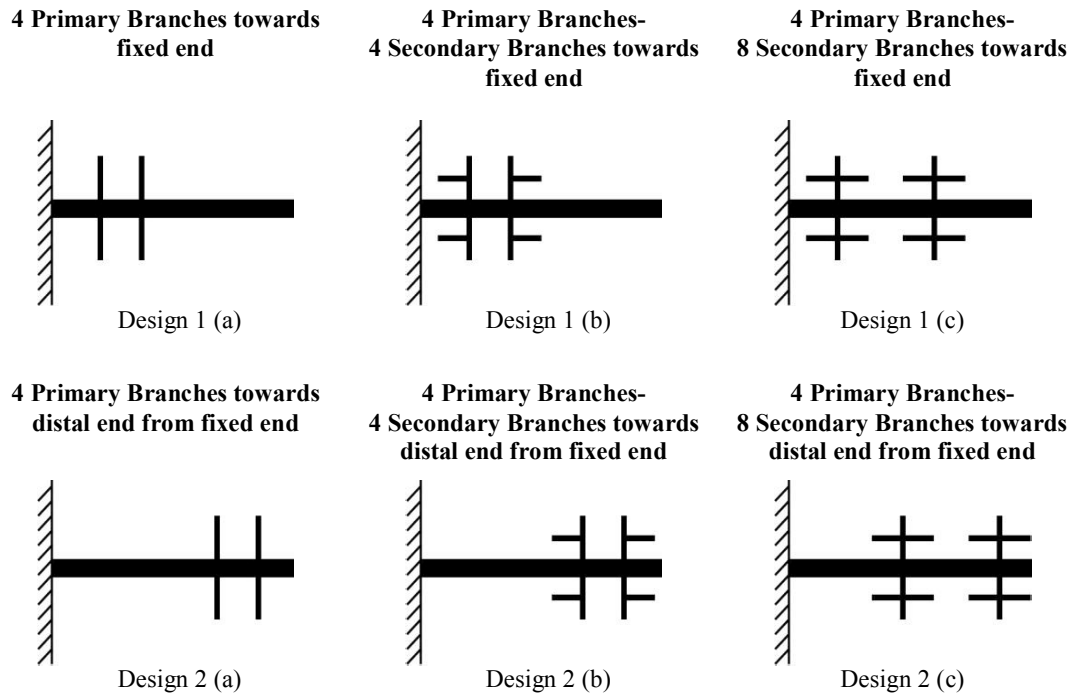

Figure 5.16: Designs of secondary branches flagellated nanoswimmer (Primary branches constant in number as 4 towards fixed end and free end of beam)

### 5.5.4   Result and discussion

A design of piezoelectric energy transduction system is simulated in COMSOL. The aim of the design is to amplify the stressing on the main flagella by doing branching on flagella surface. Both static load (branches on flagella) and dynamic load (fluidic pressure) are considered for evaluation of stresses developed on the beam. Energy transduction scheme for artificial nanoswimmer consists of 4 primary branches and number of secondary branches varies from 4 to 8. The stress and electric potential is taken towards fixed end of beam. The stress is developed on the surface of beam due to fluidic velocity applied to the inlet of outer domain to maintain low Reynolds number. The developed stress is converted into electric potential through electrostatic module coupled to piezoelectric module. The simulation results towards fixed end are plotted in Figure 5.17 for Design 1 and Design 2 (refer Figure 5.16) by varying number of secondary branches towards fixed end and free end of the beam. It is observed from the

plotted results that as number of secondary branches increase stress also increases which is being transformed into electric potential by electrostatic physics. The primary branches are kept constant but their placement varies, as towards fixed end and distal end of the beam. The von-Mises stress is found to be increased up to approximately 3097 Nm^{-2} and percentage increase in stress is 20% on increasing number of secondary branches from 4 to 8 with respect to 4 primary branches towards distal end of the beam. The von-Mises stress is transformed into electric potential by electrostatic physics and is increased 0.55 µV approximately 15%.
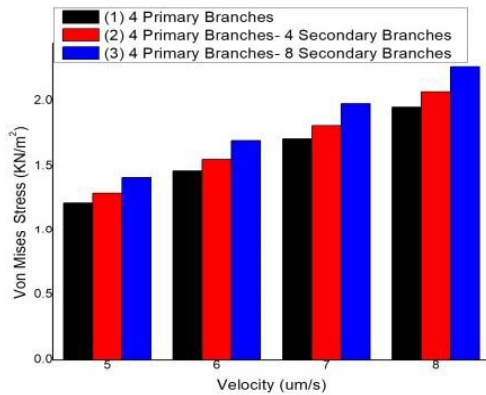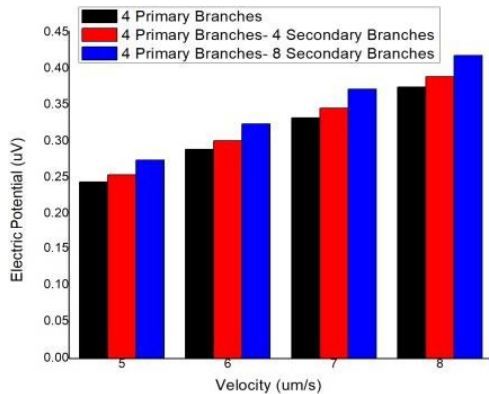

Design 1: Von Misses Stress v/s Velocity

% increase in stress- 15.84% (from 4 primary branches to 4 primary branches and 8 secondary branches).
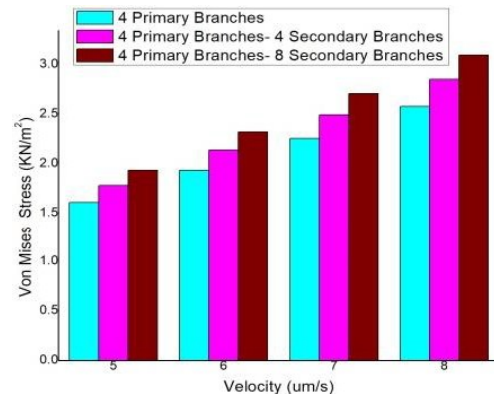
Design 2: Von Misses Stress v/s Velocity

% increase in stress- 20.09% (from 4 primary branches to 4 primary branches and 8 secondary branches).

Design 1: Electric Potential v/s Velocity

% increase in electric potential- 11.95 % (from 4 primary branches to 4 primary branches and 8 secondary branches).
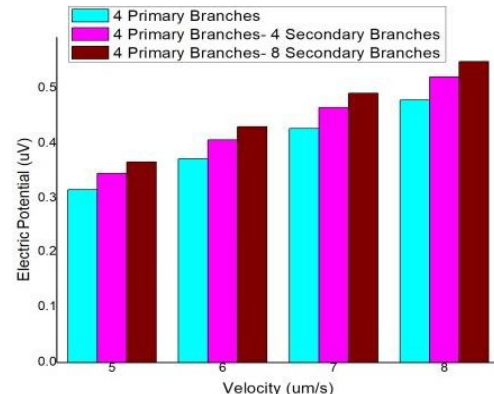
Design 2: Electric Potential v/s Velocity

% increase in electric potential- 15.23% (from 4 primary branches to 4 primary branches and 8 secondary branches).

Figure 5.17: Variation in stress and electric potential on increasing secondary branches

4 primary branched flagellated nanoswimmer is simulated and compared for increase in electric potential when placed at free end and fixed end. The assessment is done for 4 secondary branches placed at distal end (Design 1(b)) and proximal end (Design 2(b) refer Figure 5.16. The percentage increase in electric potential for COMSOL simulated result for all the designs of Figure 5.16 is represented in Figure 5.18. Maximum percentage increase in electric potential 33.71% for 4 secondary branched flagella is observed when gap between primary branches are constant (refer Figure 5.16 Design 1(b) and Design 2(b)). The secondary branched flagellated simulation results are providing enhancement in electric potential for better design of on-board energy transduction mechanism.

Percentage Increase in Electric Potential Free end - Fixed end

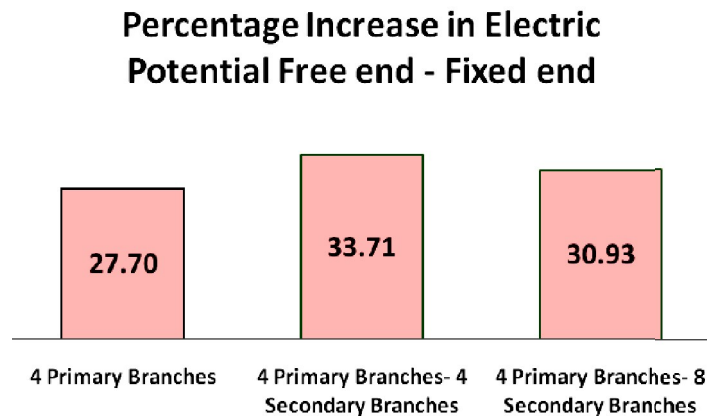| 27.70	33.71	30.93
4 Primary Branches	4 Primary Branches- 4 Secondary Branches	4 Primary Branches- 8 Secondary Branches

Figure 5.18: Percentage increase in electric potential from free end to fixed end for different designs of secondary branched flagella shown in Figure 5.16

From section 5.4 and 5.5, it is concluded that due to uniform branching on flagella surface, flagella do not get twisted along with bending because of self-loading. Branches provide the dynamic damping to the flagella by increasing the stability to the designed system and preventing the mechanical failure. If fluidic pressure is changed abruptly, there are chances of breaking artificial flagellated nanoswimmer. So, branching is done on flagella surface to provide stiffness to the design and to meet explicit mechanical necessities. Primary branches are getting mechanical strength by adding secondary branches on it and will smooth out the oscillation of primary branches. When angle of branches are deviated from 90° orientation, they become closer together and leads to weaker branch design [66], [67] of flagellated artificial nanoswimmer. Thus, 90° orientation of branches on flagella surface is most preferable for energy transduction

mechanism. Due to increase in mass loading through branches and bending of piezo based branched flagella leads to generation of increase in electric potential. Placement of branches towards free end of flagella is giving better results because more surface area is exposed as well as it is free to oscillate to produce high electric potential. In the next section, the primary branched flagellated nanoswimmer designs are studied through planar motion for electric potential development as well as energy flux generation.

5.6 Energy Harnessing of Branched Flagellated Artificial Nanoswimmer: Planar Actuation Mode

In nature, planar motion is exhibited by bacteria and mimicked in the present section through oscillatory motion. Piezoelectric based artificial nanoswimmer converts the mechanical motion produced by planar propulsion into electrical charge through direct piezoelectric effect. In the present study we compare the effect of increase in number of branches in terms of electric potential and energy flux generated. The designs of branched flagellated artificial nanoswimmer are chosen as shown in Figure 5.19 because maximum increase in electrical potential is generated for distal end branched flagella. The numbers of branches are increased from 2 to 6 on beam surface with dimensions mentioned in Table 5.7. The material is chosen as biocompatible PVDF piezoelectric material. Three modules are considered for COMSOL simulation: laminar flow and solid mechanics are coupled by fluid structure interaction multiphysics while solid mechanics and electrostatics are coupled through piezoelectric module available in multiphysics.
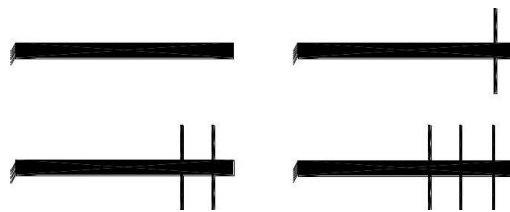

Figure 5.19: Model of unbranched and branched flagella

5.6.1 Governing equation, boundary conditions and meshing used in modeling in COMSOL

In laminar flow physics module, pressure point constraint boundary condition is set as zero initially to provide zero pressure at outer domain boundaries. No slip boundary condition is applied on all boundaries.

In solid mechanics module, the piezoelectric-strain charge constitutive equations used to study mechanical and electrical performance in COMSOL. When solid body gets deformed, internal forces get disturbed which is called as stresses. According Newton's second law, internal forces such as stress in a body along with external and inertial forces must be in balance. The momentum balance equation for solid material is given by equation (5.10)

$$\rho \frac{\partial^2 u_{solid}}{\partial t^2} = \nabla \bullet (FS)^T + f_V \tag{5.10}$$

whereas, FS is the first and second Piola-Kirchhoff stress tensor together and f_v represents the volume forces such as gravitational and centrifugal forces. The von Mises stress is calculated using equation (5.9). The partial derivatives of displacement gradient is a measure of how fast the displacement changes and so strain. The strain (ε) - displacement is given by Green-Lagrange equation (5.11)

$$\varepsilon = \frac{1}{2}\left[\left(\nabla u_{solid}\right)^T + \nabla u_{solid} + \left(\nabla u_{solid}\right)^T \nabla u_{solid}\right] \tag{5.11}$$

where, u_{solid} is the solid displacement. The electric-field is shown in terms of voltage V as represented in equation (5.12)

$$\text{Electric field: } E = -\nabla V \tag{5.12}$$

In piezoelectric layer electric field can also be calculated through Poisson's equation ρ_v shown in equation (5.13) and constitutive relation is given for electric displacement D through equation (5.14)

$$\nabla \bullet D = \rho_v \tag{5.13}$$

$$D = \varepsilon_0 \varepsilon_{rs} E + P_{pze} \tag{5.14}$$

where, D is the electric displacement, ε_0 and ε_{rs} are relative permittivity of water and PVDF piezoelectric material, E and P_{pze} are electric field and polarization vector as applied in charge conservation node. Before calculating voltage gain and deformation, pressure on the surface of piezoelectric polymer is occurring due to prescribed velocity V_y leads to polarization. In solid mechanics module prescribed velocity is applied at proximal end of beam shown below equation (5.15)

$$V_y = A\omega Sin\omega t \tag{5.15}$$

where A is the amplitude of oscillation taken as 1.25 μm and ω 25 Hz is the frequency exhibited by natural bacteria.

The ground node is implemented as boundary condition means zero potential on that particular boundary. In the present case lower surface of beam is used as ground. Floating potential node is provided to the upper surface of cantilever beam to measure energy density and electric potential on that surface. The ground and floating potential boundary chosen in the present model can be seen in Figure 5.20.
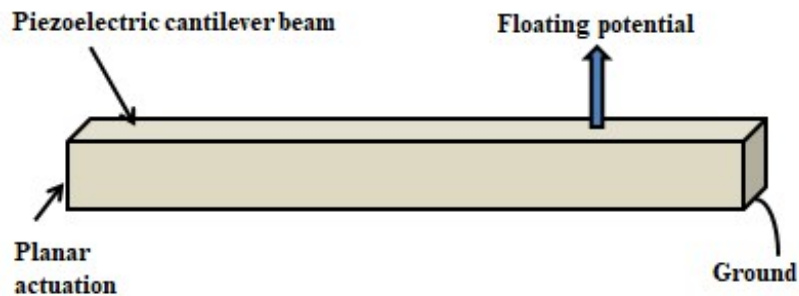

Figure 5.20: Schematic diagram of boundary conditions applied on piezoelectric modeled cantilever beam

Physics controlled mesh with element size normal is used to set mesh. It gets information from physics by which element domain and periodic condition is used automatically to provide suitable mesh sequence. For normal mesh elements for 6 branched flagellated swimmer, energy flux is noticed as 7.14 μWm^{-2}. When fine mesh is selected for 6 branches, the generated energy flux is 7.18 μWm^{-2}. Results are converging on refining the mesh but time required for computation of simulation study also increases. Approximately 0.56% increment is observed on refining the mesh size. Results are not depending on mesh size much. Time dependent study is used for computation of designed model.

5.6.2 Results and discussion

Four designs of flagellated artificial nanoswimmer are simulated to investigate on-board actuation scheme of an artificial nanoswimmer. In nature planar actuation mode is

displayed by *pantonematic* flagella, so planar actuation frequency of 25 Hz are applied at the proximal end of designed *pantonematic* flagella in terms of prescribed velocity V_y. The laminar fluid flow is maintained in the container of size 300 μm×150 μm×150 μm in which piezoelectric beam of different designs of branched flagellated artificial nanoswimmer is placed. The planar oscillation inside fluidic chamber will lead to stress generation on the flagella surface (piezoelectric cantilever beam) which in turns produce the electric potential as well as electric energy required for further actuation of designed nanoswimmer.

The simulation results are plotted in Figure 5.21 towards proximal end of flagella. The pressure on the structure is generated when oscillating at frequency 25 Hz. The resulted stress is converted into electric potential through electrostatic module. The result plotted in Figure 5.21(a), it is observed that as number of branches increase from 0 to 6 on flagella surface which is actuating at particular frequency get deformed and generate electric potential because of direct piezoelectric effect. The highest electric potential is developed for 6 branches flagellated artificial nanoswimmer approximately 1 nV and correspondingly energy flux is produced as 7.14 μWm^{-2}. There is a linear increase in electric potential value. We can increase the electric potential either by increase in actuation frequency or by investigating secondary branched flagellated nanoswimmer for energy transduction system.
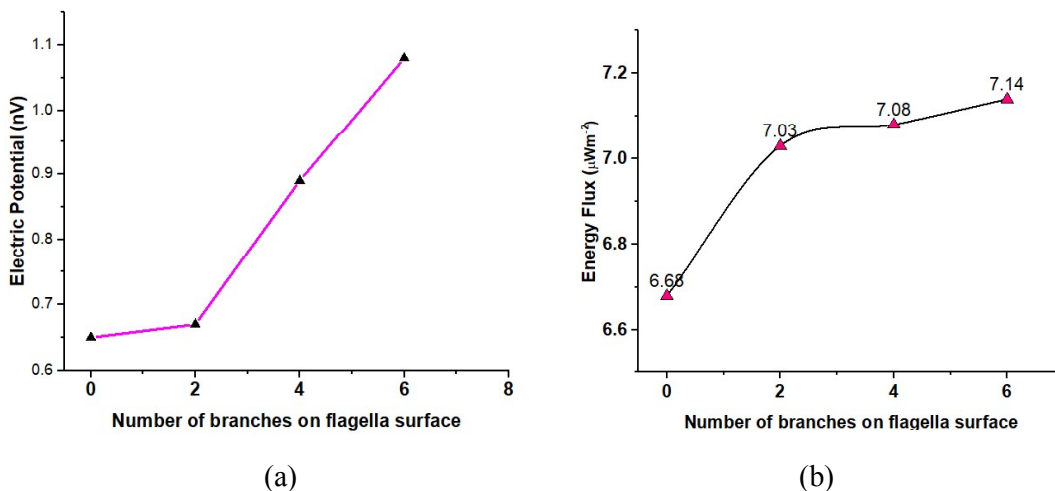

(a)   (b)

Figure 5.21: (a) and (b) showing electric potential variation and change in energy flux on increasing number of branches on flagella surface

5.7   Summary

An energy harnessing system based on piezoelectric material has been explored in last three decades but it is still a developing technology and key area of interest in nano-domain. Attractive design for actuation of artificial nanoswimmer is simulated by mimicking natural flagella and branching structure. Material chosen for actuation mechanism is PVDF which happens to be biocompatible and piezoelectric both. The conventional energy harvester such as electrostatic method require external voltage source and electromagnetic energy conversion technique needs to incorporate moving parts and provide very low output in terms of voltage. Piezoelectric based energy harnessing for artificial nanoswimmer neither involve external voltage source nor any moving parts for conversion.

1. Simulating fluid structure interaction (FSI) in COMSOL software, the performance of energy harnessing feature of artificial nanoswimmer to propel *in-vivo* environments is studied. The designs are based on the concept of harnessing energy by piezoelectric effect i.e. by stressing and then generating piezoelectric potential. Two practically relevant cases are explored; a straight fin/branch (90° orientation) attached to the beam like mastigonemes on flagella surface and branches at an angle other than 90° on flagella surface.

2. Investigation on various designs was done by adjusting parameters like velocity, number of branches, placement of branches and orientation of branches on flagella surface. It is observed that the fins at 90° orientation placed near to the free end of the beam, achieved maximum stresses and thence maximum transduction to electric potential. The design with largest number of fins at distal end of beam attained maximum stress and consequently 60.65% increase in generated electric potential in comparison to design without fins.

3. Secondary branching investigated further to study and to realize harnessing energy for an artificial nanoswimmer. Analysis shows that secondary branching increases stress and electric potential. The proposed design is used to convert mechanical energy from flowing blood into electrical energy using PVDF piezoelectric material, which helps motion of artificial nanoswimmer inside the human body for specific biological applications such as drug delivery.

4. The planar actuation is shown by natural bacteria and applied at one end of flagella and branches are present on another end of flagella such as distal end. The electric

potential generated is 1.08 nano-volts and energy flux generated is 7.14 μWm^{-2}. The values of electric potential and energy flux from PVDF based artificial nanoswimmer for design having 6 branches on flagella surface is obtained by oscillating the flagella at frequency exhibit by micro-organisms. This is a combine effort of material technology and electrical circuits, which come together to enhance conversion efficiency and to full fill energy demands of portable device such as nanorobots to make it fully self-powered.

References:

[1]   J. S. Rathore and N. N. Sharma, "Engineering nanorobots: chronology of modeling flagellar propulsion," *Journal of Nanotechnology in Engineering and Medicine*, vol. 1, no. 3, pp. 31001–31007, 2010.

[2]   B. M. Nandish and B. Hosamani, "A Review of Energy Harvesting From Vibration using Piezoelectric Material," *International Journal of Engineering Research & Technology*, vol. 3, no. 7, pp. 1607–1610, 2014.

[3]   M. C. Shinob, "Replacement Of Heart Bypass Surgery By Nanorobots," *Int. J. Adv. Res. Technol*, vol. 2, no. 3, pp. 119–122, 2012.

[4]   R. A. Freitas, "Pharmacytes: An ideal vehicle for targeted drug delivery," *Journal of Nanoscience and Nanotechnology*, vol. 6, no. 9–10, pp. 2769–2775, 2006.

[5]   R. A. Freitas Jr, "Nanodentistry.," *Journal of the American Dental Association (1939)*, vol. 131, no. 11, pp. 1559–1565, 2000.

[6]   G. Loget and A. Kuhn, "Electric field-induced chemical locomotion of conducting objects," *Nature communications*, vol. 2, pp. 535–540, 2011.

[7]   F. Lugli, E. Brini, and F. Zerbetto, "Shape governs the motion of chemically propelled janus swimmers," *The Journal of Physical Chemistry C*, vol. 116, no. 1, pp. 592–598, 2011.

[8]   L. O. Mair *et al.*, "Highly controllable near-surface swimming of magnetic Janus nanorods: application to payload capture and manipulation," *Journal of Physics D: Applied Physics*, vol. 44, no. 12, pp. 125001-125010, 2011.

[9]   L. Wang, H. Xu, W. Zhai, B. Huang, and W. Rong, "Design and characterization of magnetically actuated helical swimmers at submillimeter-scale," *Journal of Bionic Engineering*, vol. 14, no. 1, pp. 26–33, 2017.

[10]   X. Wang, J. Song, J. Liu, and Z. L. Wang, "Direct-current nanogenerator driven by ultrasonic waves," *Science*, vol. 316, no. 5821, pp. 102–105, 2007.

[11]   O. J. Sul, M. R. Falvo, R. M. Taylor II, S. Washburn, and R. Superfine, "Thermally actuated untethered impact-driven locomotive microdevices," *Applied Physics Letters*, vol. 89, no. 20, pp. 203512–203516, 2006.

[12]   L. Zhang *et al.*, "Characterizing the swimming properties of artificial bacterial flagella," *Nano Letters*, vol. 9, no. 10, pp. 3663–3667, 2009.

[13]   S. Nain and N. N. Sharma, "Propulsion of an artificial nanoswimmer: a comprehensive review," *Frontiers in Life Science*, vol. 8, no. 1, pp. 2–17, 2015.

[14]   J. M. J. den Toonder and P. R. Onck, "Microfluidic manipulation with artificial/bioinspired cilia," *Trends in biotechnology*, vol. 31, no. 2, pp. 85–91, 2013.

[15]   K. Oh, J.-H. Chung, S. Devasia, and J. J. Riley, "Bio-mimetic silicone cilia for microfluidic manipulation," *Lab on a Chip*, vol. 9, no. 11, pp. 1561–1566, 2009.

[16]   T. L. Jahn, M. D. Lanman, and J. R. Fonseca, "The mechanism of locomotion of flagellates. II. Function of the mastigonemes of Ochromonas," *The Journal of Protozoology*, vol. 11, no. 3, pp. 291–296, 1964.

[17]   R. Caliò *et al.*, "Piezoelectric energy harvesting solutions," *Sensors*, vol. 14, no. 3, pp. 4755–4790, 2014.

[18]   S. Chalasani and J. M. Conrad, "A survey of energy harvesting sources for embedded systems," in *IEEE SoutheastCon,* pp. 442–447, 2008.

[19]   R. A. Freitas, *Nanomedicine, volume I: basic capabilities*. Landes Bioscience Georgetown, TX, pp. 411-430, 1999.

[20]   P. D. Mitcheson, P. Miao, B. H. Stark, E. M. Yeatman, A. S. Holmes, and T. C. Green, "MEMS electrostatic micropower generator for low frequency operation,"

Sensors and Actuators A: Physical, vol. 115, no. 2, pp. 523–529, 2004.

[21] A. Truitt and S. N. Mahmoodi, "A review on active wind energy harvesting designs," *International Journal of Precision Engineering and Manufacturing*, vol. 14, no. 9, pp. 1667–1675, 2013.

[22] D. P. Arnold, "Review of microscale magnetic power generation," *IEEE Transactions on Magnetics*, vol. 43, no. 11, pp. 3940–3951, 2007.

[23] S. P. Beeby, M. J. Tudor, and N. M. White, "Energy harvesting vibration sources for microsystems applications," *Measurement science and technology*, vol. 17, no. 12, pp. 175–195, 2006.

[24] S. Roundy, P. K. Wright, and J. Rabaey, "A study of low level vibrations as a power source for wireless sensor nodes," *Computer communications*, vol. 26, no. 11, pp. 1131–1144, 2003.

[25] H. F. Hassan, S. I. S. Hassan, and R. A. Rahim, "Acoustic energy harvesting using piezoelectric generator for low frequency sound waves energy conversion," *International Journal of Engineering and Technology (IJET)*, vol. 5, no. 6, pp. 4702–4707, 2014.

[26] D. Vatansever, E. Siores, and T. Shah, "Alternative resources for renewable energy: piezoelectric and photovoltaic smart structures," *Global warming–impacts and future perspective*, pp. 263-290, 2012.

[27] S. R. Anton and H. A. Sodano, "A review of power harvesting using piezoelectric materials (2003–2006)," *Smart materials and Structures*, vol. 16, no. 3, pp. R1-R22, 2007.

[28] H. A. Sodano, D. J. Inman, and G. Park, "Generation and storage of electricity from power harvesting devices," *Journal of Intelligent Material Systems and Structures*, vol. 16, no. 1, pp. 67–75, 2005.

[29] Y. Gao and Z. L. Wang, "Electrostatic potential in a bent piezoelectric nanowire. The fundamental theory of nanogenerator and nanopiezotronics," *Nano letters*, vol. 7, no. 8, pp. 2499–2505, 2007.

[30] C. Chang, V. H. Tran, J. Wang, Y.-K. Fuh, and L. Lin, "Direct-write piezoelectric polymeric nanogenerator with high energy conversion efficiency," *Nano letters*, vol. 10, no. 2, pp. 726–731, 2010.

[31] J. Fang, X. Wang, and T. Lin, "Electrical power generator from randomly oriented electrospun poly (vinylidene fluoride) nanofibre membranes," *Journal of Materials Chemistry*, vol. 21, no. 30, pp. 11088–11091, 2011.

[32] I. Dakua and N. Afzulpurkar, "Piezoelectric energy generation and harvesting at the nano-scale: materials and devices," *Nanomaterials and Nanotechnology*, vol. 3, pp. 1–21, 2013.

[33] F. Mohammadi, A. Khan, and R. B. Cass, "Power generation from piezoelectric lead zirconate titanate fiber composites," in *Materials Research Society Symposium Proceedings*, vol. 736, pp. 263–270, 2003.

[34] A. Kumar, A. Sharma, R. Kumar, R. Vaish, and V. S. Chauhan, "Finite element analysis of vibration energy harvesting using lead-free piezoelectric materials: A comparative study," *Journal of Asian Ceramic Societies*, vol. 2, no. 2, pp. 138–143, 2014.

[35] R. Majumdar, N. Singh, J. S. Rathore, and N. N. Sharma, "In search of materials for artificial flagella of nanoswimmers," *Journal of Materials Science*, vol. 48, no. 1, pp. 240–250, 2013.

[36] H. H. E. Johnny and Y. F. Li, "High sensitivity piezoresistive cantilever sensor for biomolecular detection," in *Journal of Physics: Conference Series*, vol. 34, no. 1, p. 429-435, 2006.

[37] H. Li, C. Tian, and Z. D. Deng, "Energy harvesting from low frequency applications using piezoelectric materials," *Applied physics reviews*, vol. 1, no. 4, pp. 41301-41322, 2014.

[38] J. W. Sohn, S. B. Choi, and D. Y. Lee, "An investigation on piezoelectric energy harvesting for MEMS power sources," *Proceedings of the Institution of Mechanical Engineers, Part C: Journal of Mechanical Engineering Science*, vol. 219, no. 4, pp. 429–436, 2005.

[39] C. J. Kendall and P. Fisher, "Parasitic Power Collection in Shoe Mounted Devices ", pp. 1-27, 1998.

[40] G. W. Taylor, J. R. Burns, S. A. Kammann, W. B. Powers, and T. R. Welsh, "The energy harvesting eel: a small subsurface ocean/river power generator," *IEEE journal of oceanic engineering*, vol. 26, no. 4, pp. 539–547, 2001.

[41] S. Pobering and N. Schwesinger, "A novel hydropower harvesting device," in *2004 International Conference on MEMS, NANO and Smart Systems (ICMENS'04)*, pp. 480–485, 2004.

[42] H. A. Sodano, J. Granstrom, J. Feenstra, and K. Farinholt, "Harvesting of electrical energy from a backpack using piezoelectric shoulder straps," in *Active and Passive Smart Structures and Integrated Systems*, vol. 6525, pp. 652502-652513, 2007.

[43] C. Chang, Y.-K. Fuh, and L. Lin, "A direct-write piezoelectric PVDF nanogenerator," in *TRANSDUCERS 2009-2009 International Solid-State Sensors, Actuators and Microsystems Conference*, pp. 1485–1488, 2009.

[44] B. J. Hansen, Y. Liu, R. Yang, and Z. L. Wang, "Hybrid nanogenerator for concurrently harvesting biomechanical and biochemical energy," *ACS nano*, vol. 4, no. 7, pp. 3647–3652, 2010.

[45] H. Mutsuda, J. Miyagi, Y. Doi, Y. Tanaka, H. Takao, and Y. Sone, "Flexible piezoelectric sheet for wind energy harvesting," *International Journal of Energy Engineering*, vol. 4, no. 2, pp. 67-75, 2014.

[46] A. Proto *et al.*, "Using PVDF films as flexible piezoelectric generators for biomechanical energy harvesting," *Lékař a technika-Clinician and Technology*, vol. 47, no. 1, pp. 5–10, 2017.

[47] K. Li, X. Liu, Y. Liu, and X. Wang, "A piezoelectric generator based on PVDF/GO nanofiber membrane," in *Journal of Physics: Conference Series*, vol. 1052, no. 1, pp. 12110–12113, 2018.

[48] S. Nain, J. S. Rathore, and N. N. Sharma, "Comparison of Piezo-material based Energy Transduction Systems for Artificial Nanoswimmer," in *IOP Conference Series: Materials Science and Engineering*, vol. 346, no. 1, pp. 12079-12086, 2018.

[49] F. Mokhtari, J. Foroughi, T. Zheng, Z. Cheng, and G. M. Spinks, "Triaxial braided piezo fiber energy harvesters for self-powered wearable technologies," *Journal of Materials Chemistry A*, vol. 7, no. 14, pp. 8245–8257, 2019.

[50] C. Brennen and H. Winet, "Fluid mechanics of propulsion by cilia and flagella," *Annual Review of Fluid Mechanics*, vol. 9, no. 1, pp. 339–398, 1977.

[51] M. Zhu, E. Worthington, and A. Tiwari, "Design study of piezoelectric energy-harvesting devices for generation of higher electrical power using a coupled piezoelectric-circuit finite element method," *IEEE transactions on ultrasonics, ferroelectrics, and frequency control*, vol. 57, no. 2, pp. 427–437, 2010.

[52] P. A. Manoharan and D. Nedumaran, "Design and Modeling of MEMS based Nano Displacement PZT Sensing Element," *International Journal of Computer Applications*, vol. 975, pp. 34-41, 2012.

[53] A. Mineto, M. P. Braun, H. A. Navarro, and P. S. Varoto, "Modeling of a cantilever beam for piezoelectric energy harvesting," in *9th Brazilian conference on Dynamics, control and their applications, Sao Carlos, Brazil*, pp. 599–605, 2010.

[54] U. K. M. Bangi, "Development of a fluid actuated piezoelectric micro energy harvester: Finite element modeling simulation and analysis," *Asian Journal of Scientific Research*, vol. 6, no. 4, pp. 691–702, 2013.

[55] F. Lv, R. Song, X. Zhang, X. Shan, and T. Xie, "Simulation Study for Energy Harvesting Using Polyvinylidene Fluoride flag in the Flow," in *3rd International Conference on Material, Mechanical and Manufacturing Engineering (IC3ME 2015)*, pp. 1703-1709, 2015.

[56] B. Behkam and M. Sitti, "Design methodology for biomimetic propulsion of miniature swimming robots," *Journal of Dynamic Systems, Measurement, and Control*, vol. 128, no. 1, pp. 36–43, 2006.

[57] H. Hoshikawa and R. Kamiya, "Elastic properties of bacterial flagellar filaments: II. Determination of the modulus of rigidity," *Biophysical chemistry*, vol. 22, no. 3, pp. 159–166, 1985.

[58] F. Gittes, B. Mickey, J. Nettleton, and J. Howard, "Flexural rigidity of microtubules and actin filaments measured from thermal fluctuations in shape.," *The Journal of cell biology*, vol. 120, no. 4, pp. 923–934, 1993.

[59] S. T. Miller, R. L. Campbell, C. W. Elsworth, J. S. Pitt, and D. A. Boger, "An overset grid method for fluid-structure interaction," *World Journal of Mechanics*, vol. 4, no. 7, pp. 217-237, 2014.

[60] H. Guo, J. Nawroth, Y. Ding, and E. Kanso, "Cilia beating patterns are not hydrodynamically optimal," *Physics of Fluids*, vol. 26, no. 9, pp. 91901-91913, 2014.

[61] M. S. Kumar and P. Philominathan, "The physics of flagellar motion of E. coli during chemotaxis," *Biophysical reviews*, vol. 2, no. 1, pp. 13–20, 2010.

[62] E. Lauga and T. R. Powers, "The hydrodynamics of swimming microorganisms," *Reports on Progress in Physics*, vol. 72, no. 9, pp. 96601–96636, 2009.

[63] C. Brennen, "Locomotion of flagellates with mastigonemes," *Journal of Mechanochemistry and Cell Motility*, vol. 3, no. 3, pp. 207–217, 1975.

[64] G. B. Bouck, "The structure, origin, isolation, and composition of the tubular mastigonemes of the Ochromonas flagellum," *The Journal of cell biology*, vol. 50, no. 2, pp. 362–384, 1971.

[65] S. Nain, J. S. Rathore, and N. N. Sharma, "Harness enough energy for locomotion of an artificial nanoswimmer: design and simulation," in *AIP Conference Proceedings*, 2018, vol. 1989, no. 1, pp. 20032–20039.

[66] "Prepare Your Trees for a Storm," available online at http://richardstreeservice.com/about/resources/prepare-trees-for-storm.php.

[67] "Reducing Tree Damage In Future Storm" available online at https://arbor1.com/wpcontent/uploads/2013/09/reducingtreedamageinfuturestorms.pdf, pp. 1.